Surface & Coatings Technology 480 (2024) 130595

Contents lists available at ScienceDirect

Surface & Coatings Technology

journal homepage: www.elsevier.com/locate/surfcoat

Full length article

New nanoscale multilayer magnetron sputtered Ti-DLC/DLC coatings with improved mechanical properties

Mobeen Haneef [a,b,*], Manuel Evaristo [a], Ardian Morina [b], Liuquan Yang [b], Bruno Trindade [a,*]

[a] University of Coimbra, CEMMPRE – Centre for Mechanical Engineering Materials and Processes, ARISE - Advanced Production and Intelligent Systems, Department of Mechanical Engineering, Rua Luís Reis Santos, 3030-788 Coimbra, Portugal
[b] Institute of Functional Surfaces (iFS), School of Mechanical Engineering, University of Leeds, LS2 9JT, Leeds, United Kingdom

ARTICLE INFO

Keywords:
DC magnetron sputtering
Monolayer and multilayer coatings
Ti-doped DLC coatings
Mechanical properties
Adhesion
Nanometric period

ABSTRACT

Two sets of nanoscale multilayer Ti-DLC/DLC coatings, with similar chemical composition but different periods between consecutive layers (0.4 and 5.5 nm), were deposited by non-reactive direct current magnetron sputtering using different rotational speeds of the substrate holder (12 and 1 rpm, respectively) in this work. The results show that the overall Ti content in the coatings varied from ≈ 2.9 to ≈ 8.2 at. % in both cases. Significant fluctuations in the Ti concentration between the middle points of the DLC and Ti-DLC layers were observed for the coatings deposited at 1 rpm. All the coatings deposited were mainly amorphous, presenting a columnar structure and a cauliflower-like granular surface morphology. The sp^2/sp^3 ratio increased as the concentration of Ti rose. The coatings deposited at 1 rpm demonstrated better mechanical properties (up to 33 % improvement in hardness and up to 25 % improvement in the elastic modulus) when compared to the equivalent coatings deposited at 12 rpm. The multilayer titanium doped coating (deposited at 1 rpm) with 5.9 at. % Ti presented the most significant improvement in mechanical properties when compared to pure DLC and monolayer coatings deposited at 12 rpm. The results confirmed that it is possible to tune the performance of this type of coatings by depositing alternating layers of pure DLC and Ti-doped DLC.

1. Introduction

DLC (diamond-like carbon) coatings, first developed by Schmellenmeier in 1953 [1], are amorphous carbon structures with sp^2 (graphite-like) and sp^3 (diamond-like) bonded carbon atoms [2]. The proportion of sp^2 and sp^3 determines the properties of the DLC. These coatings have been generally produced by physical vapour deposition (PVD) processes such as filtered cathodic vacuum arc (FCVA) [3–7], pulsed laser deposition (PLD) [8–11], and sputtering [12–18] to achieve different properties. The DLC coatings are usually deposited on the Si and the metal-based substrates to facilitate the different characterisation techniques. The Si substrate is used where a freshly cut cross-section or a smooth surface is required in order to perform the analysis, e.g., to avoid oxidation and contamination during SEM and EDS analysis. Metal-based substrates are used to evaluate the adhesion strength and to evaluate tribological properties of the coatings with the substrate of interest according to the application, in our case, AISI M2 steel.

In general, the titanium-doped coatings deposited by FCVA and PLD show high rates of hardness and internal stresses compared to those deposited by sputtering. Concerning sputtering, different power supplies and configurations have been used including: direct current (DC) magnetron sputtering [19], high-power impulse magnetron sputtering (HiPIMS) [20], and radio frequency (RF) sputtering [21], to name a few. Among these, non-reactive DC magnetron sputtering (DCMS) has been the most widely used technique for depositing DLC coatings. This technique has the benefit of using a noble gas, which is used as the active gas to generate plasma. The ions from the plasma bombard the target, and the material ejected from it is deposited on the substrate. When compared with the other DLC deposition techniques, DCMS is an economical deposition method and can easily be scaled up from the laboratory to production. Moreover, this technique is environmentally friendly due to the use of a noble gas and electricity only, which makes it a green technology for the production of such coatings.

DLC coatings have been applied to automobile engine components including fuel injectors, wrist pins, tappets, journal bearings, ball bearings, and roller bearings [22], where low COF and wear rates are

* Corresponding author at: University of Coimbra, CEMMPRE – Centre for Mechanical Engineering Materials and Processes, ARISE - Advanced Production and Intelligent Systems, Department of Mechanical Engineering, Rua Luís Reis Santos, 3030-788 Coimbra, Portugal.
E-mail addresses: mobeen.haneef@dem.uc.pt, mnmhan@leeds.ac.uk (M. Haneef).

https://doi.org/10.1016/j.surfcoat.2024.130595
Received 20 June 2023; Received in revised form 16 October 2023; Accepted 23 February 2024
Available online 28 February 2024

required. However, DLC coatings show some thermal instability at increasing temperatures [23,24]. To overcome this issue, non-metallic elements: (hydrogen, boron, nitrogen, phosphorus, silicon, fluorine, and sulphur) [25,26], metals: (copper, nickel, tungsten, titanium, molybdenum, chromium, and niobium) [27–29], and oxide nanoparticles of transition metals [30] have been incorporated in DLCs. The incorporation of these elements or compounds has also been reported as a way to reduce the internal stresses of DLC coatings [31].

Titanium-doped DLC (Ti-DLC) coatings have been frequently studied for tribological applications. These coatings induce a higher thermal stability of the DLC up to 450 °C [32], a reduction in the internal stresses [33], an elevated reactivity with additives in lubricating oils [34], and a reduced coefficient of friction in un-lubricated and lubricated conditions [35]. However, the addition of Ti to DLCs leads to some detrimental effects on mechanical properties, such as a decrease in hardness and a poorer adhesion to the substrates [33]. Most of the literature on Ti-doped DLC coatings refers to very high or very low amounts of Ti [3–9,11,13–18]. Therefore, there is a need to study DLC coatings with Ti concentrations between 0 and 10 at. % deposited by DCMS. The literature reports deposition of micrometric layered Ti-DLC coatings with layered structures of DLC/Ti [36], Ti/Ti-DLC [3], Ti-DLC/TiC [9], DLC/TiC [37], and sp^2/sp^3 [38,39].

Aside from multilayer structures of DLC coatings involving titanium, some research works have also reported multilayer structures of a-C/a-C:H [40] DLC coatings, but mechanical properties were not studied. Kim et al. [41] deposited multilayer DLC coatings composed of a-C:H:W/ a-C:H for tribological applications without investigating the effect of the layers on the mechanical properties of the coatings.

No studies on the deposition of nanoscale multilayer magnetron sputtered Ti-DLC/DLC coatings have been reported in the literature.

This investigation aimed to develop a new strategy to manufacture DLC coatings doped with different percentages of Ti by DCMS without negatively affecting the mechanical properties of DLC. The strategy adopted consisted of depositing alternating layers of DLC and Ti-doped DLC with nanometric periods. By varying the substrate rotations, two sets of coatings with similar chemical compositions (≈ 2.9, ≈ 6.1, and ≈ 8.3 at. %) but with different nanometric layer periods/cycles were produced. The morphological, structural, and mechanical results obtained for these two kinds of coatings are presented, compared, and discussed.

2. Experimental details

Pure DLC and Ti-doped DLC coatings were deposited on quenched and tempered AISI M2 steel (H = 63 HRC) obtained from Thyssenkrupp Materials Iberica and (100) ± 0.5° monocrystalline silicon substrates from Siegert Wafer. Before the depositions, the AISI M2 samples were cleaned with acetone to remove the oxidation-inhibiting sticky oil. They were polished by means of Struers Planopol-3 equipment, using silicon carbide abrasive papers till 1200 mesh and a 3 μm diamond suspension on a Struers MD/DP-Nap cloth. After polishing, the M2 and silicon substrates were rinsed in an Equiultra ultrasonication equipment bath with acetone, ethanol, and distilled water for 15 min in each medium, respectively. An average 60 and 0.8 nm roughness were measured by atomic force microscopy (AFM) for the polished AISI M2 samples and Si substrate, respectively.

The coatings were deposited in TEER equipment UDP 650/4 with one chromium (99.95 % pure) and three graphite targets (380 mm × 175 mm and 99.99 % pure) from PhotonExport, placed at 90° to each other (Fig. 1a). In one of the graphite targets, fourteen Ti (99.90 % pure) pellets from Testbourne Ltd. were embedded in CNC machined holes (20 mm diameter and 5 mm deep) (Fig. 1b).

Two different rotational speeds (1 and 12 rpm) of the substrate holder were used for the deposition of coatings with different periods/cycles between the DLC and Ti-DLC layers. For the higher rotational speed (12 rpm), multilayer coatings with very short periods were produced (from now on, referred to as monolayer *m*Ti-DLC coatings). For 1 rpm, multilayer coatings (*M*Ti-DLC coatings) with a higher period were produced.

A chromium and carbon gradient interlayer (≈ 0.3 μm thick) was deposited to enhance the interfacial adhesion between the coatings and the substrates. The concentration of chromium in the interlayer varied from 100 % closest to the substrates to 0 % at the top. This was achieved by initially applying a 110 V negative bias to the substrate and 2000 W to the chromium target for 10 min. After this time, the power at the chromium target was reduced from 2000 W (current of 5.7 A) to 0 W for another 10 min. Simultaneously, the power at the two pure graphite targets was increased from 0 to 1750 W (current of 2.9 A). The schematic of the two methodologies used is shown in Fig. 2. It is worth mentioning that in the multilayer coatings, there is no discrete boundary between DLC and Ti-DLC layers because of the rotation of substrates in front of targets; that is why the term period(s)/cycle(s) are used.

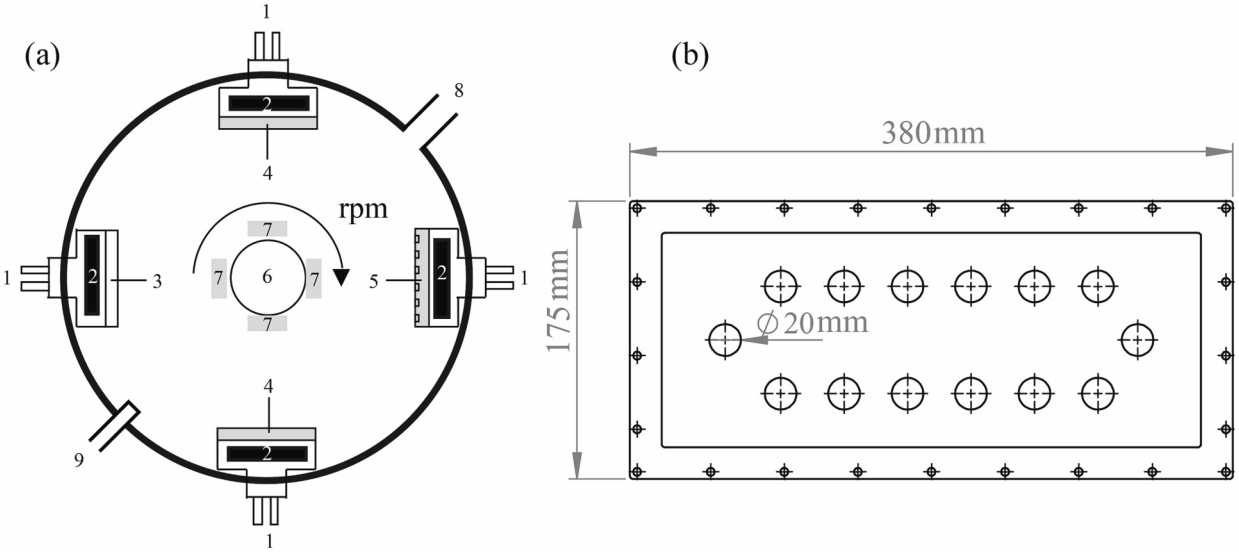

Fig. 1. The sputtering system: (a) positioning the targets (380 mm × 175 mm) and the rotating substrate holder (1 = cooling system, 2 = magnets, 3 = chromium target, 4 = graphite targets, 5 = graphite + Ti target, 6 = rotatable substrate holder, 7 = substrates, 8 = vacuum pump, 9 = Ar flow), and (b) composite graphite target with 14 Ti pellets (20 mm in diameter × 5 mm thick) embedded in CNC machined holes.

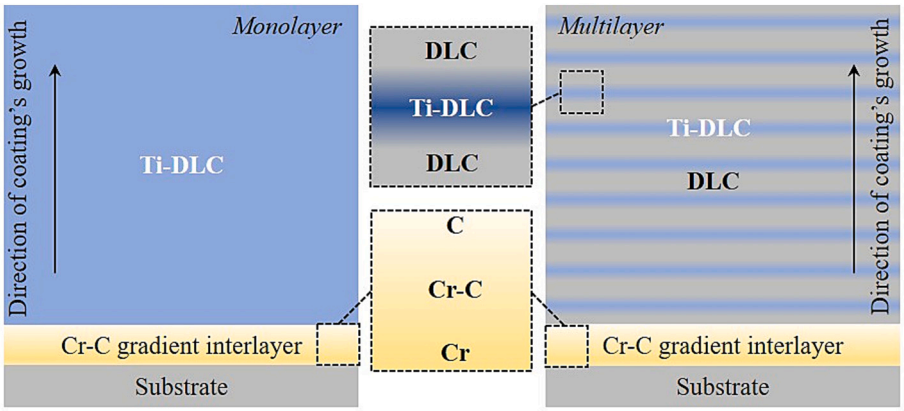

Fig. 2. Schematic of the two methodologies used for the deposition of the coatings: Ti-DLC (monolayer *m*Ti-DLC), and Ti-DLC/DLC (multilayer *M*Ti-DLC) coatings.

Before deposition of the coatings, the sputtering chamber was evacuated down to an ultimate base pressure of ≈ 1.0×10^{-6} mBar. Argon gas was used as the active/working gas for sputtering at a working pressure of ≈ 1.1×10^{-3} mBar. Before the depositions, the targets were sputter-cleaned for 15 min using Argon and -600 V bias; during this time, the targets were covered with a shutter. The AISI M2 steel and monocrystalline Si substrates were also surface cleaned by argon plasma simultaneously as the targets were being cleaned. The cleaning of substrates took place by applying a -600 V bias to the substrates by a pulsed DC power source.

The nomenclature of the coatings deposited and the main deposition parameters are shown in Table 1. One pure DLC coating (named DLC), three monolayer *m*Ti-DLC and three multilayer *M*Ti-DLC coatings were deposited. Three different power values of 150 W (current of 0.48 A), 335 W (current of 0.93 A), and 500 W (current of 1.27 A) were applied to the composite (graphite + Ti) target to deposit coatings with different atomic concentrations of Ti. The power at the pure graphite targets was kept constant at 1750 W (current of 2.9 A). Since the sputtering yield of Ti is higher than that of graphite, lower deposition times were selected for higher powers to obtain coatings with identical thicknesses.

Crystallographic analysis of the DLC coatings was performed by x-ray diffraction (XRD - Panalytical X'pert) with cobalt radiation (kα = 1.78897 Å) in Bragg Brentano geometry from 30° to 60° (2θ). Grazing incidence analysis was also performed with an incident angle of 2° to avoid interference from the Cr—C interlayer and Si substrate. The morphology and the thickness of the coatings were assessed by field emission electron microscopy (FEI-SEM – Hitachi, Merlin Gemini III). The elemental compositional analysis was performed by energy dispersive spectroscopy (EDS - Oxford Instruments). Rutherford backscattering (RBS) and elastic recoil detection analysis (ERDA) measurements were performed at the SIAM platform in Belgium. RBS was carried out in normal incidence, using an alpha beam at 4.3 MeV for sensitivity to carbon. The backscattered particles were collected by 2 detectors set at 135° and 165° with respect to the incident beam direction. The samples were tilted at 70° and analysed with an alpha beam at 2.3 MeV, with a detector set at 30° relative to the incident beam direction to quantify the hydrogen. RBS was used with mainly two purposes: to confirm the EDS results and to quantify the amount of hydrogen in the coatings. Their internal structure was observed by transmission electron microscopy (FEI-TEM - Titan Themis Cubed 300 TEM). The cross-sectional samples for TEM analysis were prepared by a focused ion beam (FIB – ThermoFisher, FEI Helios G4 CX DualBeam).

The Ti concentration in the DLC/Ti-DLC layers of the coatings was assessed by TEM-EDS. The NEXAFS (near-edge X-ray absorption fine structure) C K-edge spectra were measured for the energy range of 280–320 eV to quantify the sp^2 and sp^3 content in the coatings. NEXAFS was performed using BL-29 BOREAS beamline at ALBA synchrotron in Spain. The coatings were analysed with beamline energies from 280 to 320 eV while using the drain current as a signal. A highly ordered pyrolytic graphite (HOPG) sample was used as a reference due to its pure graphite characteristics (100 % sp^2 [42]). The sp^2 content was measured using the isolated peak of 1 s → π* resonance transition, in which one electron from the 1 s orbital of carbon is excited to the unoccupied π* orbital. This transition takes place at 285 eV for pure graphite and it is the characteristic peak of sp^2 (C═C) hybridised bonded carbon atoms [43]. The chemical bonding in the multilayer coatings was analysed by X-ray photoelectron spectroscopy (XPS - EnviroESCA equipped with an Al *kα* x-ray source). When using the XPS first, a survey scan was performed from 800 to 0 eV, and then individual peak scans were performed from 298 to 278 eV and 470–450 eV for C 1 s and Ti 2p,

Table 1
Nomenclature of the coatings deposited and main deposition parameters.

Sample		Power at the graphite + Ti target (W)	Power at the graphite targets (W)	Deposition time (min)	The rotational speed of the substrate holder (rpm)
DLC	DLC	–	1750	376	12
*m*Ti-DLC1	Monolayer Ti-DLC	150	1750	350	12
*m*Ti-DLC2		335	1750	318	12
*m*Ti-DLC3		500	1750	300	12
*M*Ti-DLC1	Multilayer Ti-DLC/DLC	150	1750	350	1
*M*Ti-DLC2		335	1750	318	1
*M*Ti-DLC3		500	1750	300	1

m = monolayer, *M* = multilayer.

respectively. During the XPS analysis three scans were obtained for every spectrum, with a pass energy of 50 eV, and an energy step size of 0.1 eV. The deconvolution of C1s XPS experimental spectra was performed using CasaXPS software [44].

The hardness (H) and reduced modulus (E*) were measured by nanoindentation (Micro Materials Ltd., NanoTest) with a Berkovich indenter. The tests were performed on DLC coatings deposited on Si substrates, the equipment was operated in the load control mode. Sixteen tests were performed on each sample under a load of 5 mN. This load was selected in such a way that the indenter did not penetrate the coatings more than 10 % of their thickness; this was confirmed manually from statistical data. The values of H/E^*, H^3/E^{*2} and W_e were calculated. The former two parameters reflect the elastic/plastic properties [45], and the latter represents the toughness and resistance to cracking [46,47] of the coatings. The higher the W_e, the higher the toughness of the coating is. The W_e values were calculated from the following equation [48].

$$W_e = \left[\frac{(d_{max} - d_{res})}{d_{max}}\right] \times 100\% \quad (1)$$

Where d_{max} is the maximum indentation depth during loading and d_{res} is the residual indentation depth after unloading.

The adhesion of the coatings to the M2 substrates was assessed using a scratch test (CSEM Revetest), according to ASTM C1624-22 [49]. The loads corresponding to the first delamination of the coatings (Lc2 - adhesive failure) were determined by micrographs of the scratches and close inspection of the cracking and delamination. Five tests were performed on each sample for a load range of 0–50 N, and a length of 5 mm (10 N/mm) using a Rockwell-C indenter. The scratches were analysed by a travelling optical microscope (Leica LH 111 LED).

The residual stresses were calculated from the coatings on the silicon substrates by means of a stylus profilometer (Mitutoyo, Surftest SJ-500) and employing the Stoney equation [50].

$$\sigma = \frac{E_s}{6(1 - V_s)} \frac{hs^2}{hf} \left(\frac{1}{R} - \frac{1}{R_0}\right) \quad (2)$$

Where *Es,* Vs, and *hs* are the Young's modulus, the Poisson's ratio and the thickness of the substrate, respectively, *hf* is the thickness of the coating, and R_0 is the value of the radius of curvature of the substrate before deposition, and *R* is the value of the radius of curvature of coating deposited on the same substrate for which R_0 was measured.

3. Results and discussion

3.1. Morphological, chemical, and structural analysis

The SEM images of the cross-sections and surfaces of the DLC, *m*Ti-DLC1, *m*Ti-DLC3, *M*Ti-DLC1, and *M*Ti-DLC3 coatings are shown in Fig. 3.

The Cr—C gradient interlayer, the undoped DLC, and the Ti-doped DLC coatings exhibited a cross-section columnar morphology. The columns were better defined and more continuous in the coatings richer in titanium. The surface of the coatings presented a typical granular cauliflower-like morphology related to the so-called atomic shadowing effect [51]. This effect may originate from obliquely incident atoms being preferentially deposited on the hills of the surface, and it can occur even during normal angle deposition. It leads to a long-range geometrical effect. The substrate holder was rotating during the depositions in this study.

Consequently, the growth of the coatings occurred with oblique deposition of C and Ti species during a significant part of the deposition. It is reported in the literature that the size of the granules depends on the substrate bias, substrate temperatures, working pressure, and the number of incident particles [52]. The substrate bias was kept constant (−110 V) for all the depositions. However, the increase in the titanium

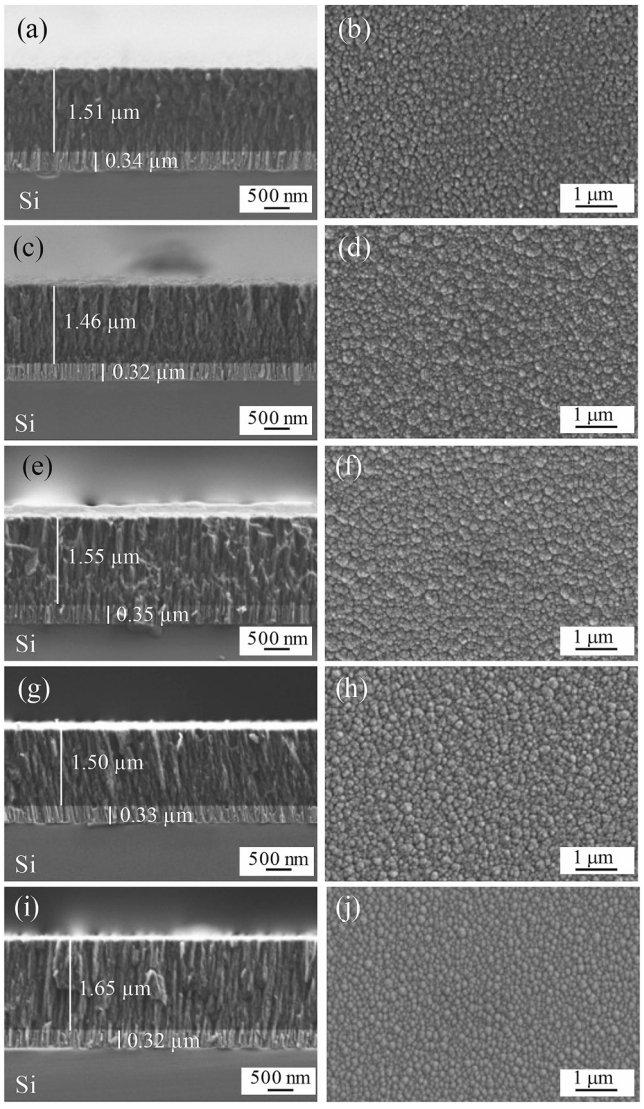

Fig. 3. SEM images of the cross-section (left) and surface (right) of the coatings. (a, b) DLC, (c, d) *m*Ti-DLC1, (e, f) *m*Ti-DLC3, (g, h) *M*Ti-DLC1, and (i, j) *M*Ti-DLC3.

content in the coatings induced an increase in the size of the granules. This can be explained by the fact that titanium has a higher sputtering yield than carbon, and therefore, a large number of incident particles were adsorbed and accumulated on the surface, which resulted in large-sized granules [53].

The thicknesses of the Cr—C gradient interlayer and the DLC-based coatings were similar for all the depositions, with mean values of ≈ 0.33 and ≈ 1.55 µm, respectively. The DLC coating was deposited with the rotational speed of 12 rpm for 376 min, corresponding to a sputtering rate of 4.0 nm/min (0.33 nm/revolution). Since two graphite targets were used in this deposition, each target was responsible for the deposition of about 0.17 nm of DLC per revolution. As the power applied to the graphite targets was the same for all the depositions (1750 W), it was possible to calculate the contribution of the graphite + Ti target towards the overall thickness of the Ti-DLC layers deposited per revolution (Fig. 4), based on the total thickness of the doped-DLC coatings, and the sputtering time. As expected, the cumulative thickness per revolution differed for the *m*Ti-DLC and *M*Ti-DLC coatings. Values close to 0.4 and 4 nm were calculated for these coatings, respectively. For both types of coatings, the thickness of the Ti-DLC layers increased as the power applied to the graphite + Ti target was increased (higher

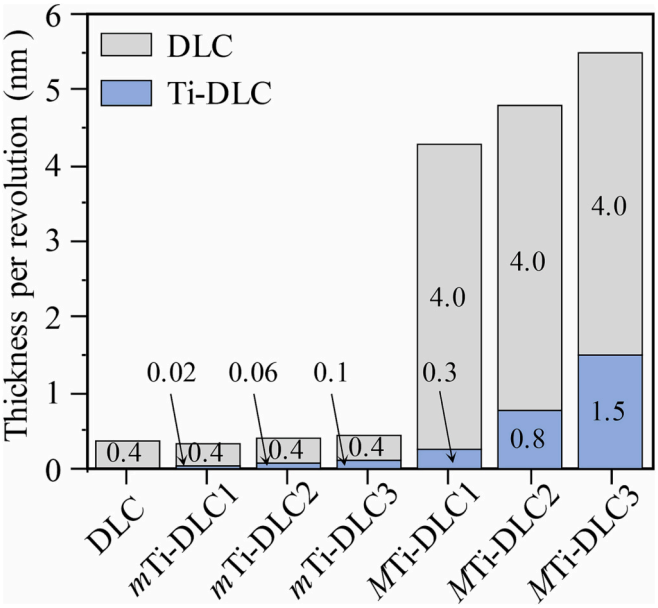

Fig. 4. Thickness of DLC and Ti-DLC layers per revolution for the DLC, *m*Ti-DLC, and *M*Ti-DLC coatings.

sputtering yields of C and Ti at higher power), while for DLC, there was no change because of the constancy of the power applied. Fig. 4 represents the contribution of graphite and graphite + Ti targets towards thicknesses achieved as per the deposition rates and rotational speeds of the substrate holder, hence not to be confused with the structure and period of layers.

The elemental compositional results assessed by SEM-EDS and ERDA-RBS are shown in Table 2.

It is evident from the results that Ti was incorporated into the DLC coatings in different amounts. EDS and ERDA-RBS analyses show analogous Ti compositions. The amounts of hydrogen in the coatings varied from 0.2 to 0.7 at. %, which may have originated from the leftover water vapour after the generation of the vacuum. It should be noted that even with a high vacuum, there is always a certain amount of water vapour in the deposition chamber.

Similar overall chemical compositions were obtained for the *m*Ti-DLC and *M*Ti-DLC coatings deposited with the same power applied to the graphite + Ti target. The SEM-EDS values presented in Table 2 were obtained with the same electron beam energy, and therefore, the interaction volume of the electron beam was of the same order for the monolayer and multilayer coatings. The EDS analysis was performed on the surface of the coatings on an area of ≈ 5500μm^2 and at a magnification of 1000×. One coating (*M*Ti-DLC44) was deposited with just the graphite + Ti composite target (no power applied to the pure graphite targets), with the same parameters used for the deposition of the *M*Ti-DLC3 coating, to determine the Ti chemical composition in the *M*Ti-DLC layers. A Ti concentration of 44 at. % was measured for this coating by EDS. Based on this value, and assuming a linear relationship between the power applied to the graphite + Ti target and the Ti concentration in both monolayer and multilayer Ti-DLC coatings, the mean Ti concentrations in the Ti-DLC layers of the *M*Ti-DLC1 and *M*Ti-DLC2 were estimated based on the EDS results (15 and 32 at. %, respectively) (Fig. 5). It can be concluded that the *M*Ti-DLC coatings showed important fluctuations in Ti concentrations between the centre of the DLC and Ti-DLC layers, due to the lower rotational speed of the substrate holder.

Table 2
Chemical composition of the coatings assessed by SEM-EDS and ERDA-RBS.

Coating	SEM-EDS (at. %)				ERDA-RBS (at. %)			
	C	Ti	Ar	O	C	Ti	Ar	H
DLC	96.3	0.0	3.4	0.3	94.3	0.0	5.0	0.7
*m*Ti-DLC1	94.2	2.9	2.7	0.2	*	*	*	*
*m*Ti-DLC2	90.6	6.1	2.9	0.4	*	*	*	*
*m*Ti-DLC3	88.2	8.3	2.5	0.4	*	*	*	*
*M*Ti-DLC1	93.0	2.9	3.4	0.7	93.1	3.1	3.5	0.3
*M*Ti-DLC2	90.5	5.9	3.2	0.4	*	*	*	*
*M*Ti-DLC3	87.9	8.2	3.3	0.6	87.3	8.5	4.0	0.2

*Not measured.

The XRD phase identification (θ-2θ diffraction mode) of the Si substrate, Cr—C gradient interlayer, pure DLC, and Ti-doped DLC coatings is presented in Fig. 6. The XRD grazing analysis did not give additional information, and therefore, the results are not shown.

The silicon substrate presented a crystalline peak at 2θ = 38.6°, ascribed to the (200) plane of the silicon face-centred-cubic structure (fcc) (ICDD card 80-0018). The (111) plane of this structure, which should be placed at 2θ = 33.2°, is absent, meaning a crystallographic orientation along the direction [200]. The Cr—C interlayer is crystalline with a diffraction peak at 52.3°, ascribed to the (110) plane of the body-centred-cubic (bcc) structure of chromium (ICDD card 85–1336). No diffraction peaks were detected from the undoped DLC coating, meaning that it was amorphous. Concerning the *m*- and *M*-Ti-DLC coatings, no additional diffraction peaks were detected. However, the *M*Ti-DLC44 (44 at. % Ti) coating showed two diffraction peaks at 2θ = 41.5° and 48.6°, assigned to the (111) and (200) planes of the fcc TiC structure (ICDD card 003-1213), respectively, with a lattice parameter of 3.66 Å. As stated in the Ti—C phase diagram, this phase may exist as a stable structure for at. % C in the range 40–50 at. %. The formation of TiC in the Ti-doped DLC coatings has been reported in the literature by different authors. In a recent work on the influence of different metals on the structural properties of co-sputtered DLC films [54] the authors, based on the XPS results, reported the formation of the TiC phase for a Ti-DLC coating with 10 at.% Ti. Besides this phase, TiO_2 was also referred to as being formed, resulting from the high concentration of oxygen in the coating (17 at. %). In another study on the microstructure, mechanical and tribological properties of multilayer Ti-DLC thick films produced by FCVA technology [55], the authors claimed that a nanocrystalline TiC phase was formed in the coatings produced with low C_2H_2 flow rates (titanium concentrations from 8.98 and 10.42 at. %). Similar to the work performed by Yetim and co-authors [54], the presence of the TiO_2 phase in the coatings was also reported.

In the present study, contrary to the *M*Ti-DLC44 coating, those deposited from both the graphite and graphite + Ti targets (monolayer and multilayer coatings) did not show diffraction peaks of the TiC phase. This apparent discrepancy can be explained by the deposition conditions used and the period of the layers. The *M*Ti-DLC44 coating was composed only of Ti-DLC layers, sputtered from the graphite + Ti target, while the *m*- and *M*-Ti-DLC coatings were formed by DLC and Ti-DLC layers with different periods. Since the *m*-Ti-DLC coatings were deposited at a higher rotational speed (12 rpm), the average period of the layers was lower compared to the multilayer coatings deposited at a lower speed (1 rpm). In order to confirm the values calculated shown in Fig. 4, TEM analysis was performed for the *M*Ti-DLC1, *M*Ti-DLC2, and *M*Ti-DLC3 coatings. The results are presented in Fig. 7, where the symbol 'Γ' represents the period or cycle between layers.

From Fig. 7 (a), (b), and (c)), the presence of the DLC and Ti-DLC layers in these coatings was clear, in particular for the coatings with higher Ti concentrations (higher periods). This was confirmed by EDS analysis (Figs. 7 (d) to (i)). In all cases, the different layers are nanometric in thickness. Mean values of 3.3 ± 1.3, 5.2 ± 0.2, and 5.6 ± 0.2 nm were obtained for the periods of the *M*Ti-DLC1, *M*Ti-DLC2 and *M*Ti-DLC3 coatings, respectively, confirming the estimated results shown in Fig. 4. The lower period of the *M*Ti-DLC1 as compared to *M*Ti-DLC2, and *M*Ti-DLC2 as compared to *M*Ti-DLC3, can be explained by the decrease in the thickness of the Ti-DLC layers with the reduction of the power applied to the graphite +Ti target because of the decreased sputtering rates of C and Ti. The multilayer coatings *M*Ti-DLC1, *M*Ti-DLC2, and

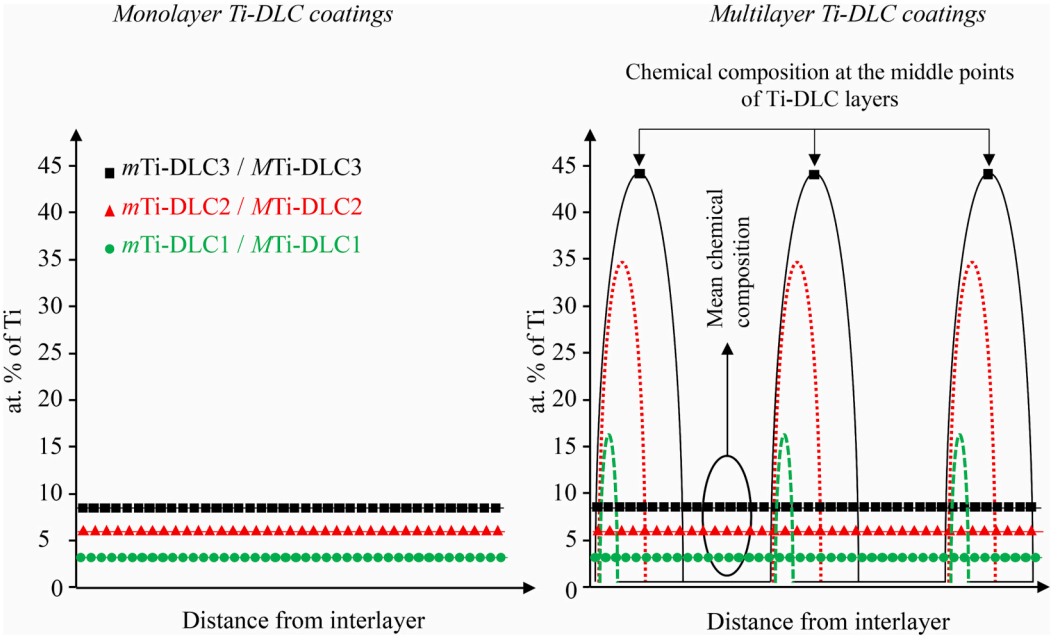

Fig. 5. Distribution of Ti in the mTi-DLC and MTi-DLC coatings. The solid lines with marks correspond to the experimental results and the dashed lines correspond to the estimated ones, based on the EDS results of the Ti-DLC coatings.

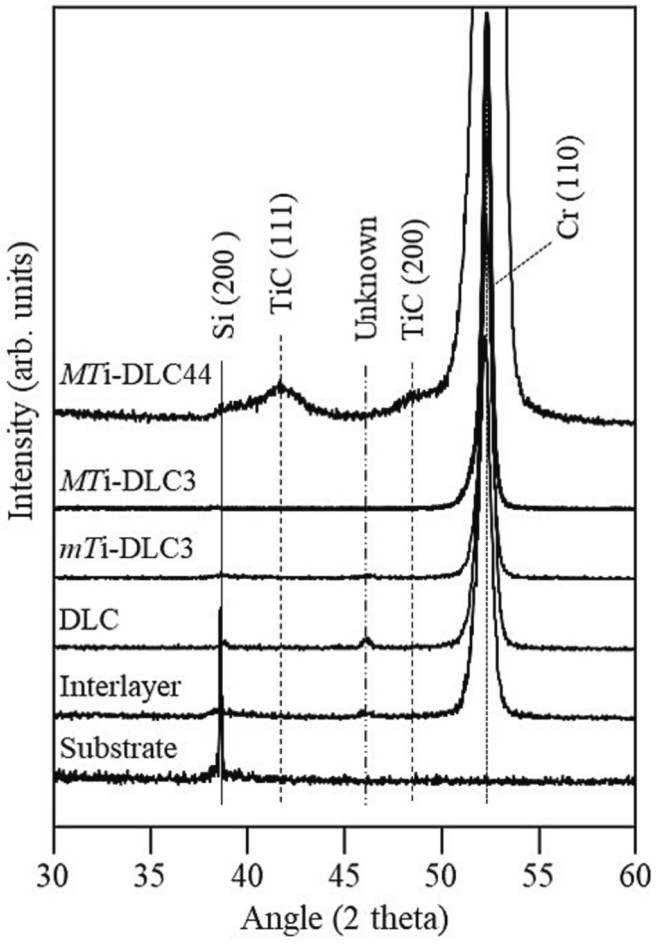

Fig. 6. X-ray diffraction patterns of the Si substrate Cr—C gradient interlayer, DLC, mTi-DLC, and MTi-DLC coatings (Co Kα radiation, θ-2θ mode).

*M*Ti-DLC3 had ≈698, ≈656, and ≈600 total layers; half were DLC and half were Ti-DLC layers.

The SAEDPs of the multilayer coatings revealed the characteristic halo ring pattern of amorphous structures, confirming the XRD results. No rings or spots ascribed to the crystalline TiC phase were detected, confirming that all the *m*- and *M*Ti-DLC coatings are mainly amorphous. The previous studies carried out regarding the SAED of DLC and Ti-DLC coatings indicate the same results about the amorphousness of these coatings [56,57].

The normalised C K-edge NEXAFS spectra of the DLC, *M*Ti-DLC1 and *M*Ti-DLC3 coatings are plotted in Fig. 8. In the same figure, the spectrum of graphite (HOPG) is also presented as a reference and the energies ascribed to the transitions from 1 s to different orbitals are indicated by dashed vertical lines.

The sharp peak at 292 eV in HOPG is ascribed to the transition where an electron is excited from the 1 s orbital of carbon to a vacant state in σ* orbital. This transition does not give a sharp appearance to the DLC-based coatings because of their non-crystalline nature. A broadband from 290 to 315 eV was observed for these coatings, ascribed to the superimposed transition of 1 s → σ* at sp^2 and sp^3 levels. The percentage of graphite in the HOPG sample was first calculated by dividing the area under the curve for the energy range 282–286.55 eV by the area under the curve for 290–315 eV to determine the sp^2 and sp^3 contents of the DLC, *M*Ti-DLC1 and *M*Ti-DLC3 coatings. Then, the percentage of graphite-like (sp^2) content was calculated by following the same procedure as for HOPG. Finally, the percentage of graphite in the coatings was divided by the percentage of graphite in HOPG, which resulted in the value of sp^2 content. The sp^3 content was calculated by subtracting the sp^2 percentage from one hundred. The curves were fitted with symmetrical peaks for the calculation of the area under the curve. The fittings of the curves corresponding to the transitions from the 1 s to the π* orbitals are shown in Fig. 9.

The peak assignment of these transitions is presented in Table 3, together with the sp^2 and sp^3 calculated percentages.

The sp^2/sp^3 ratio increased with the growth in Ti concentration, meaning that the incorporation of Ti caused graphitisation of the DLC films by acting as a catalyst during the formation of the sp^2 sites [58]. Saikubo et al. [58] studied 55 individual DLC coatings, including hydrogen-free DLC (a-C) and DLC coatings containing different amounts

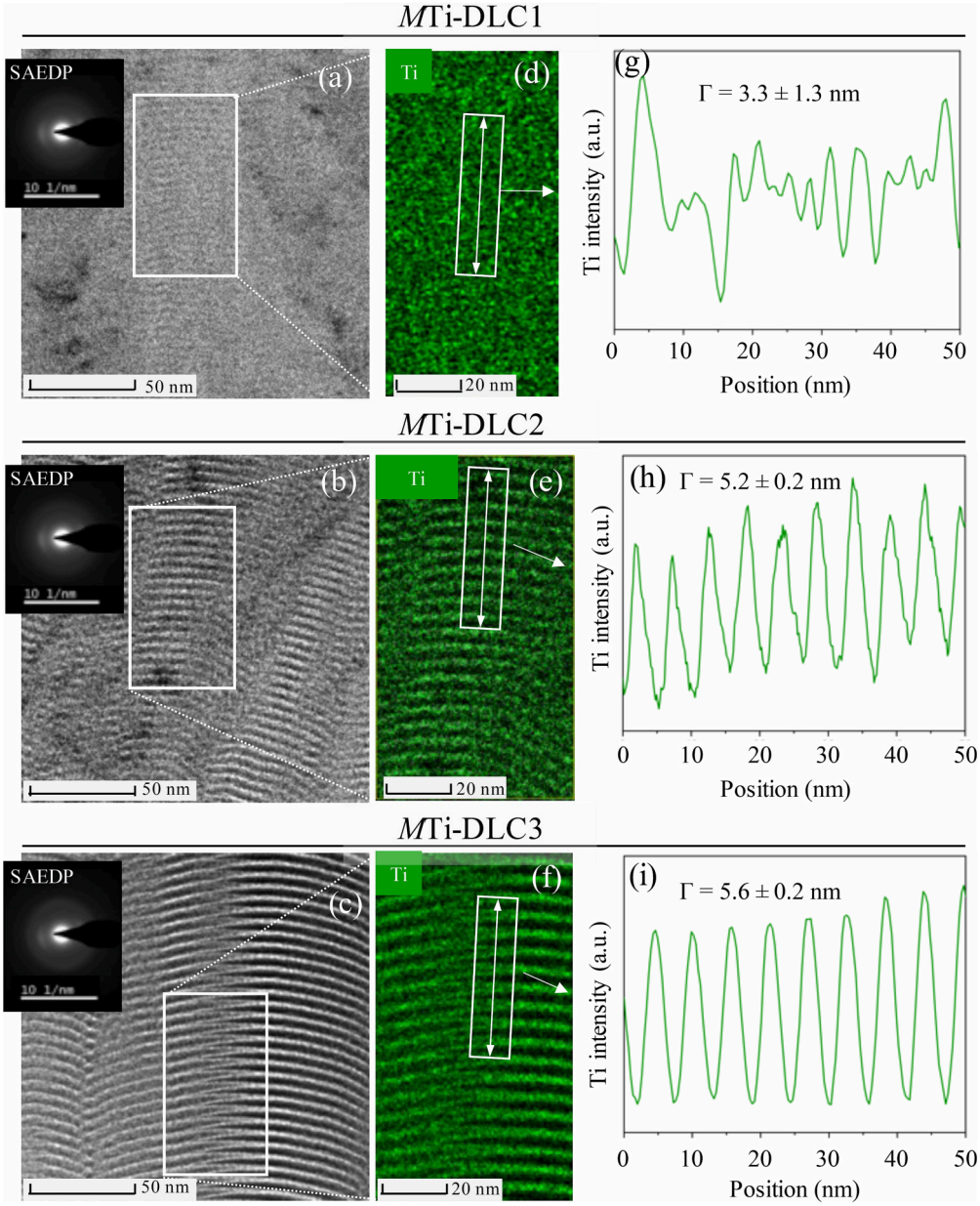

Fig. 7. TEM analysis of the multilayer *M*Ti-DLC1, *M*Ti-DLC2, and *M*Ti-DLC3 coatings. (a, b, c) high-resolution TEM images and selected area electron diffraction patterns (SAEDPs), (d, e, f) EDS maps, and (g, h, i) Ti intensity along the EDS line scans shown in (d), (e), and (f), respectively.

of hydrogen (a-C:H). The aim was to analyse the coordination of carbon atoms in the DLC and to determine the sp^2 and sp^3 percentages; the reported results agree with the ones obtained in in our study for pure DLC coating. Kanda et al. [59] studied the effect of oxygen incorporation in Ti-DLC coatings. The quantification of sp^2 and sp^3 bonded carbon was coherent with results from other studies on Ti-doped DLC coatings [55,60]. The authors also used the C K-edge spectra for measurement of sp^2 and sp^3 amounts in pure DLC. The results obtained were similar to the ones of our study.

An XPS analysis was performed to analyse the chemical bonding in the *M*Ti-DLC coatings. The Ti 2p XPS spectra are shown in Fig. 10a and the deconvoluted C 1 s spectra are shown in Figs. 10 (b to d) for the *M*Ti-DLC1, *M*Ti-DLC2 and *M*Ti-DLC3 coatings. The C 1 s spectra were deconvoluted into three sub-peaks assigned to the sp^2-bonded C—C, sp^3-bonded C—C, and C—O bonds. The Ti 2p spectra are superimposed to compare the results. Different intensities corresponding to the Ti—O and Ti—C bonds were detected in all the multilayer coatings. Taking into account the deposition geometry used and the fact that the average depth of analysis for an XPS measurement is just a few nanometres, it is difficult to draw conclusions based on the intensity or area under the peaks of Ti—O and Ti—C bonds. As the coatings produced are formed by layers of DLC and DLC + Ti with nanometric periods, the composition of the outer layer could not be confirmed, that is whether it is formed by pure DLC or Ti-doped DLC. The Ti—O and C—O bonds might result from the exposure of the coating to oxygen before carrying out the XPS analysis. It is possible to state that the Ti and C bonded atoms were present in the amorphous phase based on the electron diffraction analysis where no crystalline domains were observed and the fact that Ti—C bonds were detected by XPS spectra. This corroborates the calculations presented in Fig. 4, in which the maximum thickness of the Ti-DLC layers was 1.5 nm for the *M*Ti-DLC3 coating.

The deconvolution of the C 1 s XPS spectra (Figs. 10 b to d) showed that carbon exists in the *M*Ti-DLC coatings for the sp^2 (284.5 ± 0.2 eV) and sp^3 (285.2 ± 0.2 eV) bonding configurations [55]. The intensity of the sp^2-bonded carbon increased and the intensity of sp^3-bonded carbon decreased with the growth of the amount of titanium, which further

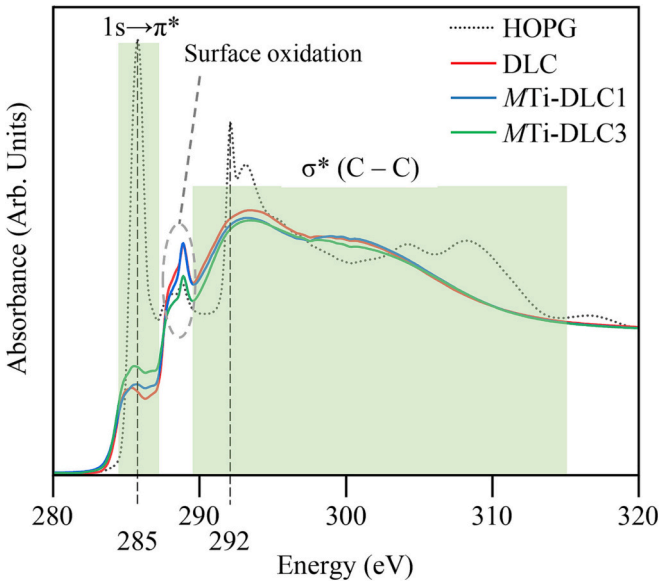

Fig. 8. NEXAFS results of the DLC, MTi-DLC1, and MTi-DLC3 coatings.

confirmed the results of NEXAFS [60,61].

3.2. Mechanical properties

The mechanical properties of the DLC, *m*Ti-DLC, and *M*Ti-DLC coatings and their residual stresses are presented in Table 4. The sp^2/sp^3 ratios obtained by NEXAFS are also included for discussion of the results.

The average values of hardness and reduced modulus for the pure DLC coating were 16.2 GPa, and 185 GPa, respectively. These values were in complete agreement with the reported literature on undoped DLC coatings deposited by DCMS [62,63]. When titanium (three different concentrations) was incorporated in the DLC to form *m*Ti-DLC and *M*Ti-DLC coatings, its effect on hardness and reduced modulus values was different for monolayer and multilayer coatings. All the *m*Ti-DLC coatings showed lower hardness as compared to pure DLC. However, when the effect of Ti dopant is discussed within the *m*Ti-DLC set of coatings without relating them with pure DLC, the values of hardness increased with the increasing amount of dopant, i.e., for Ti concentrations from 2.9 at. % to 8.3 at. % the values of hardness increased from 10.2 GPa to 12.9 GPa. For these coatings, the reduced modulus values followed the same trend as the hardness, i.e., they increased from 120.0 GPa (2.9 at.% Ti) to 152.7 GPa (8.3 at.% Ti). Feng et al. [64] reported the same results as our study, which were supported by the formation of TiC in the Ti-doped DLC coatings. In our case, the crystalline TiC was not detected because of the very short period between layers of DLC and Ti-DLC. Likewise, the results of our research and some other studies reported that incorporating metallic elements like Ti in DLC coatings can deteriorate the mechanical properties because they reduce the sp^3 content in the DLC coatings [10,15,53]. Aside from the reduction in sp^3 content due to the incorporating of Ti in the DLC coatings, other studies assign the decrease in hardness and reduced modulus to the stress-relieving effect in DLC by Ti doping [65]. Also, the reduction in the hardness and reduced modulus was justified by the fact that Ti has lower hardness and reduced modulus than that of pure DLC, and its inclusion

Table 3
Values of the sp^2 and sp^3 contents in the DLC, *M*Ti-DLC1, and *M*Ti-DLC3 coatings (C K-edge NEXAFS results).

Coating	sp^2 (%)	sp^3 (%)	sp^2/sp^3
DLC	38.8	61.2	0.63
*M*Ti-DLC1	43.2	56.8	0.76
*M*Ti-DLC3	50.6	49.4	1.02

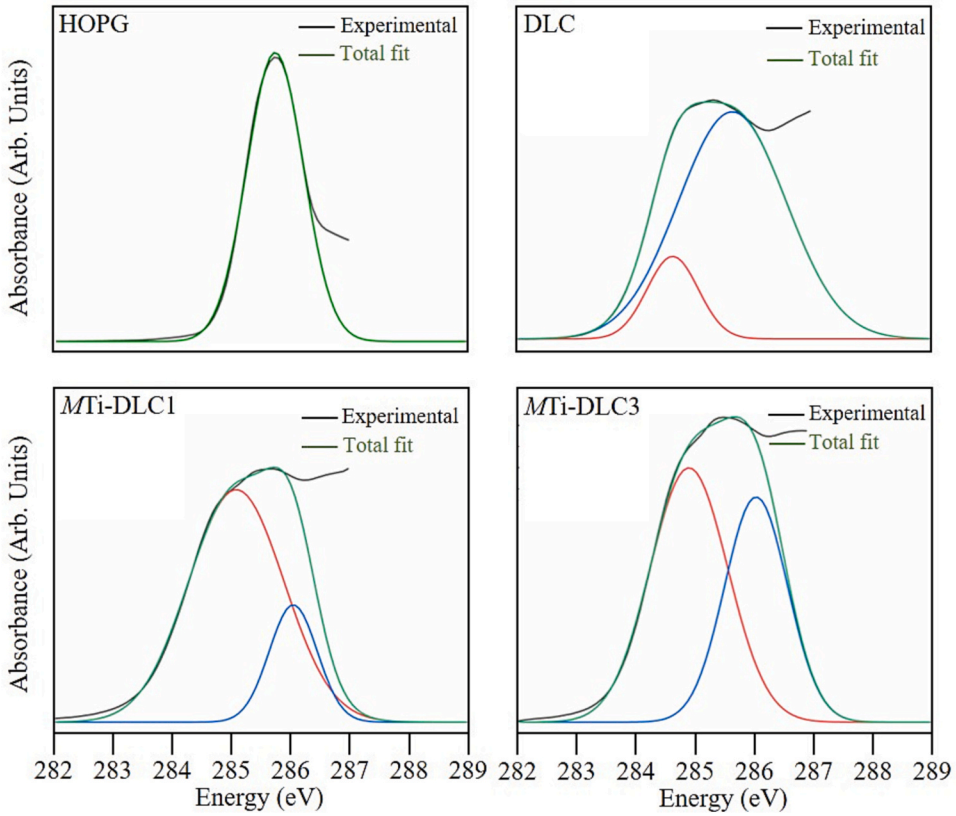

Fig. 9. Peak fitting of the normalised C K-edge NEXAFS spectra in the energy range from 282 to 289 eV for the DLC, *M*Ti-DLC1 and *M*Ti-DLC3 coatings.

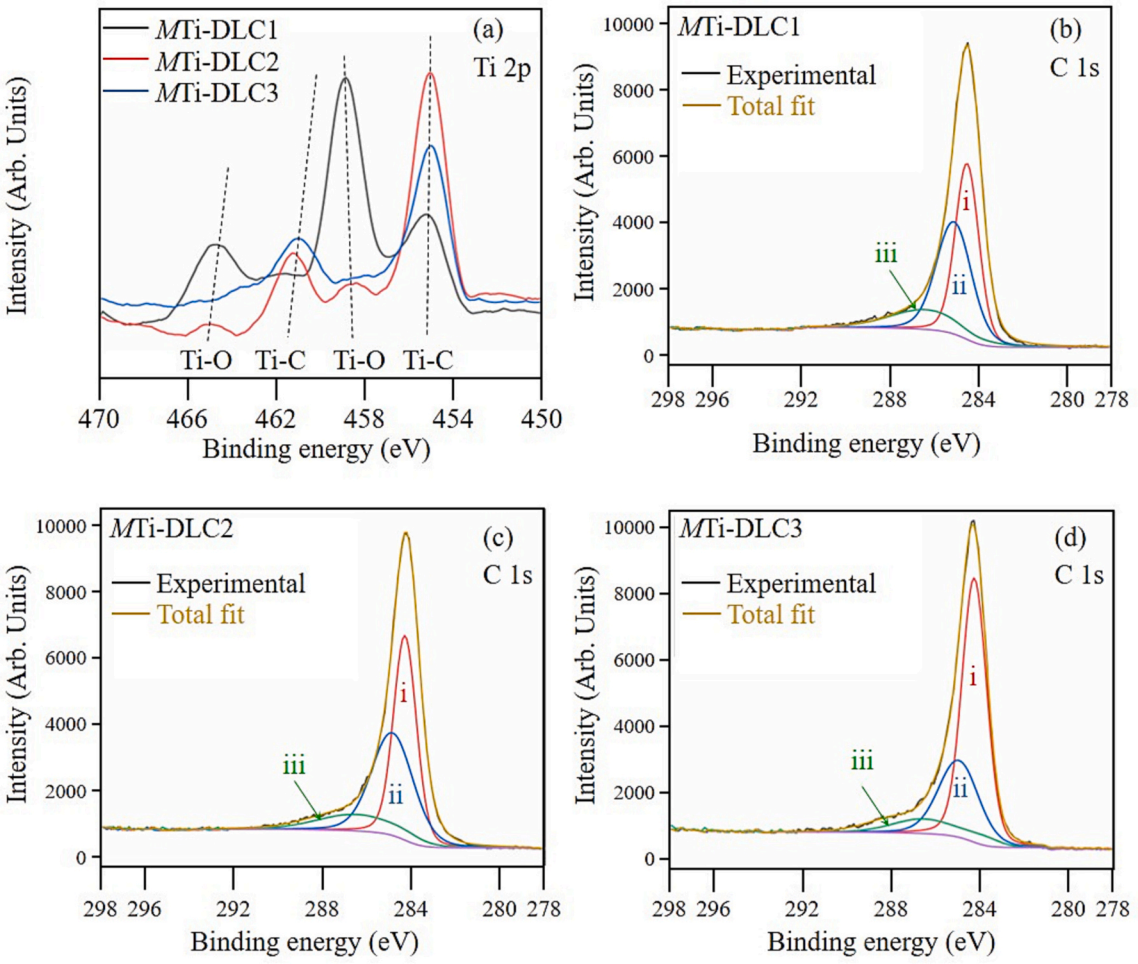

Fig. 10. (a) Ti 2p and (b), (c), and (d) C 1 s XPS spectra of the *M*Ti-DLC1, *M*Ti-DLC2 and *M*Ti-DLC3 coatings, respectively. C 1 s XPS spectra were deconvoluted into three sub-peaks assigned to the sp^2 C—C (i), sp^3 C—C (ii), and C—O bonds (iii).

Table 4
Values of the mechanical properties (H, E*, H/E*, and H^3/E^{*2}), sp^2/sp^3, and residual stresses of the coatings produced in this work.

	Ti (at. %) EDS	H (GPa)	E* (GPa)	W_e (%)	H/E*	H^3/E^{*2} (GPa)	sp^2/sp^3	Residual stresses (GPa)
DLC	0.0	16.2 ± 0.65	184.8 ± 5.9	63.9	0.087	0.123	0.63	−1.15 ± 0.07
*m*Ti-DLC1	2.9	10.2 ± 0.81	120.0 ± 5.4	68.7	0.082	0.068	*	−1.05 ± 0.05
*m*Ti-DLC2	6.1	11.8 ± 0.87	136.2 ± 7.3	70.8	0.086	0.087	*	−1.24 ± 0.03
*m*Ti-DLC3	8.3	12.9 ± 1.18	152.7 ± 9.9	67.9	0.084	0.093	*	−1.54 ± 0.16
*M*Ti-DLC1	2.9	13.3 ± 1.13	151.7 ± 7.5	67.8	0.087	0.101	0.76	−1.46 ± 0.02
*M*Ti-DLC2	5.9	15.7 ± 1.53	170.5 ± 6.6	72.5	0.092	0.132	*	−1.66 ± 0.01
*M*Ti-DLC3	8.2	12.7 ± 0.93	147.8 ± 6.1	66.0	0.085	0.093	1.02	−0.61 ± 0.02

* Not measured.

in DLC [62,63,66].

When PVD techniques are considered, Ti-doped DLC coating's hardness and elastic modulus depend on the deposition method and the parameters used. When the FCVA method was used for the deposition of Ti-DLC coatings, those coatings showed hardness values from 22 GPa to 55 GPa [3], 24 GPa to 49 GPa [4,5], and 33 GPa to 34.5 GPa [6,7]. These values were associated with the precipitation of the crystalline TiC nanometric phase in the amorphous carbon of DLC, use of very high substrate bias of up to -400 V, different duty cycles, and mainly to high residual stresses. Concerning the deposition of Ti-DLC coatings by PLD (PVD technique) [8–11], hardness values from 20 GPa to 36 GPa are reported depending on the concentration of Ti. The higher hardness of PLD-deposited Ti-DLC coatings when compared to the Ti-DLC coatings deposited by DCMS is explained by their higher sp^3 content and higher residual stresses, reaching up to −7.2 GPa. When the Ti-DLC coatings deposited by FCVA and PLD are compared with Ti-DLC coatings deposited by DCMS, the coatings deposited by DCMS presented lower hardness values in the range of 15–25.2 GPa and lower compressive stress, which were in the range of −0.1 GPa to −1.95 GPa [13,14,16–18].

Although very high hardness values were achieved for Ti-DLC coatings deposited by FCVA and PLD methods, their adhesion with the substrates was reduced to a great extent. Ti-DLC coatings deposited by the DCMS method showed better adhesion with the substrates. When Lc2 values of practical adhesion are considered, the Ti-DLC coatings deposited by FCVA showed adhesion in the range of 15–22 N [5], and the coatings deposited by PLD showed values between 3 and 11 N [8,11]. Now, coming towards discussing the adhesion of Ti-DLC coatings by DCMS, they showed better adhesion towards the substrates when compared to adhesion values of Ti-DLC coatings deposited by FCVA and

PLD. The adhesion of Ti-DLC coatings deposited by DCMS is reported in the range of 5–41 N [13–16,18]. The coatings deposited in this work showed Lc2 adhesion of 16.5–23.5 N, which agrees with the literature and is discussed in the coming section.

When discussing the trend of hardness values for *M*Ti-DLC coatings, they behaved differently as compared to *m*Ti-DLC coatings. Firstly, all the *M*Ti-DLC coatings showed lower hardness values and reduced modulus compared to the pure DLC. When comparing the hardness and

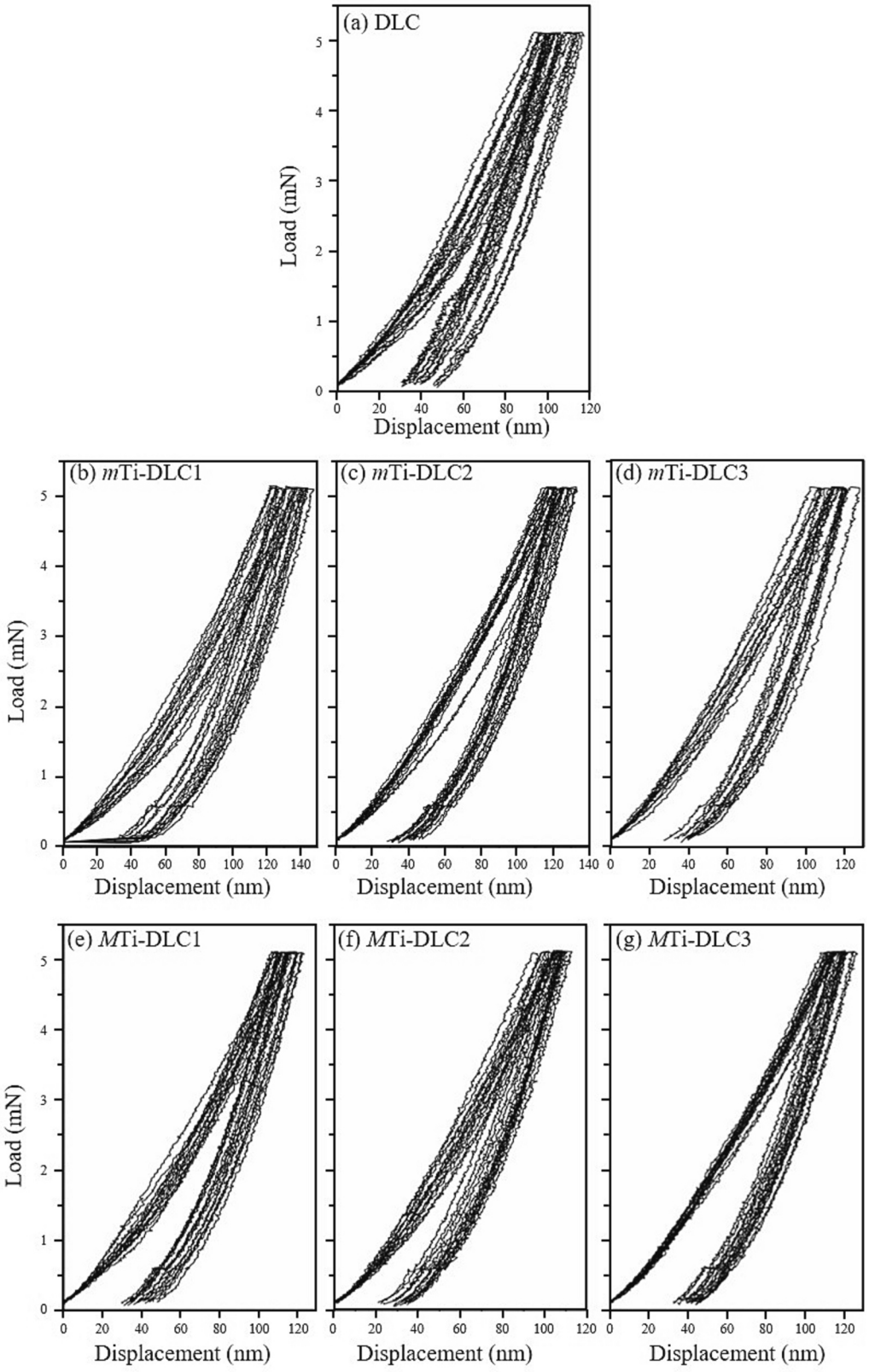

Fig. 11. Load vs displacement curves resulted from nanoindentation hardness test for (a) DLC, (b) *m*Ti-DLC1, (c) *m*Ti-DLC2, (d) *m*Ti-DLC3, (e) *M*Ti-DLC1, (f) *M*Ti-DLC2, and (g) *M*Ti-DLC3.

reduced modulus trend within the set of three *M*Ti-DLC coatings, an increase in hardness and reduced modulus was observed from *M*Ti-DLC1 (2.9 at. % Ti) to *M*Ti-DLC2 (5.9 at. % Ti). However, a decrease in hardness and reduced modulus values was observed when moving from *M*Ti-DLC2 (5.9 at. % Ti) towards the richest Ti-doped multilayer coatings *M*Ti-DLC3 (8.2 at. % Ti). Although the literature on multilayer Ti-DLC coatings with the period between layers in the nanometric range is scarce, Liu et al. [15] reported the same phenomenon for carbon (sp^2-C:Ti/sp^3-C:Ti) nano-multilayer films with sequential sp^3-rich and sp^2-rich layers deposited by DC magnetron sputtering, i.e., a hardness inflexion point for a titanium concentration of 11 at. % of Ti was observed (5.9 at. % Ti in our work). This inflexion threshold point depends mainly on the period between DLC and Ti-DLC layers, but also on the concentration of the dopant, the nature and type of dopant, the deposition system and parameters used.

The *M*Ti-DLC2 coating had the highest mechanical properties of all the Ti-doped DLC coatings (H = 15.7 and E* = 171 GPa), with values similar to the ones of pure DLC (3.2 % and 8.4 % lower than pure DLC, for hardness and reduced modulus, respectively). On the contrary, the *m*Ti-DLC1 presented 59 % and 54 % less hardness and reduced modulus values, respectively, compared to pure DLC.

The load vs displacement curves for hardness measurements by nanoindentation method are presented in Fig. 11.

The H/E and H^3/E^{*2} values, which are representative of the elastic/plastic properties of the coatings and, as explained in [45], followed the same trend as H and E*. The *M*Ti-DLC2 coating presented even higher values of H/E* and H^3/E^{*2} than the DLC coating.

Concerning W_e, all the Ti-doped coatings showed higher values than the pure DLC coating; *M*Ti-DLC2 was the toughest coating.

All the coatings produced exhibited compressive stresses due to the mismatch of thermal expansion between the DLC coatings ($\sim 2.3 \times 10^{-6}$ °C) and the substrate ($\sim 11.0 \times 10^{-6}$ °C). It is known that the residual stresses also depend on the coating's thickness (eq. 2). The thickness of the coatings produced varied from 1.46 μm to 1.65 μm (Fig. 3). Although the values of stresses were calculated from the coating thicknesses measured by SEM, some calculations were performed for each coating considering the two thicknesses mentioned above, which showed that the only variance in the values was in the second decimal point.

The mechanical properties of the Ti-doped coatings showed a direct dependence on the compressive residual stresses. Concerning the monolayer coatings, the increasing addition of titanium led to higher residual stresses and H^3/E^{*2} ratios (Fig. 12 a). Regarding the multilayer coatings, the same relationship was observed (Fig. 12 b). However, an inflexion point was observed for 5.9 at. % of Ti for multilayer coatings.

Based on these results, it can be inferred that the mechanical properties of the coatings produced in this work are mostly related to the period of the different layers, their chemical composition and residual stresses, and less to the sp^2/sp^3 ratio. The monolayer *m*Ti-DLC coatings are formed by sublayers with thicknesses lower than 0.4 nm (Fig. 4). Because *m*Ti-DLC coatings are deposited at 12 rpm of the substrate holder, the Ti dopant was distributed very uniformly within the structure of these coatings. The incorporation of Ti in the amorphous DLC structure led to its distortion due to the difference in sizes of the Ti and C atoms (0.147 and 0.070 nm, respectively). Because of the uniform distribution of Ti in monolayer coatings and the difference in sizes of Ti and C atoms, compressive stresses increased as the concentration of Ti in *m*Ti-DLC coatings increased. However, the increase in the compressive residual stresses was not linear, as explained by Xu et al. [67]. As the compressive stresses increased, the hardness and reduced modulus increased linearly.

The multilayer *M*Ti-DLC coatings are formed by the sublayers with thickness reaching 4.0 nm for DLC layers and 1.5 nm for Ti-DLC layers. Because the *M*Ti-DLC coatings were deposited at 1 rpm of the substrate holder, the distribution of Ti dopant in the DLC layers was not uniform as opposed to the *m*Ti-DLC coatings. When the Ti concentration was

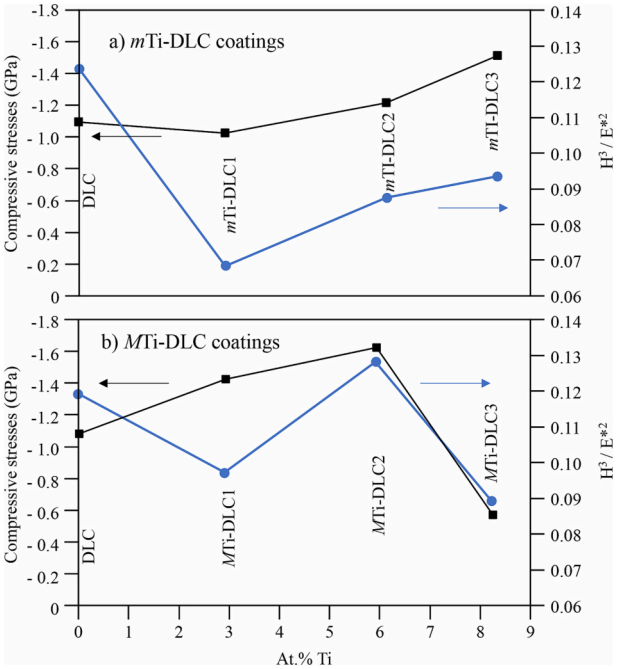

Fig. 12. Residual compressive stress and H^3 / E^{*2} of (a) *m*Ti-DLC and (b) *M*Ti-DLC coatings as a function of the Ti concentration.

increased from 2.9 at. % to 5.9 at. %, the residual compressive stresses increased because of the difference in sizes of C and Ti atoms, but this increase was much more substantial as compared to monolayer coatings because of high Ti concentration within the Ti-DLC layers, as evident from Fig. 7. For the *M*Ti-DLC coatings, when Ti concentration was increased from 5.9 at. % to 8.2 at. % the magnitude of compressive residual stress was decreased. This decrease can be explained by a very high concentration of Ti (44 at. % as illustrated in Fig. 5 and explained in subsequent section to Fig. 5) at the middle points of Ti-DLC layers and coarsening of the structure [18]. The *M*Ti-DLC coatings showed a one-to-one correspondence between mechanical properties and compressive residual stresses. Therefore, the increase in the compressive residual stresses as a function of the increase in Ti is the main factor responsible for the improvement in the mechanical properties of these coatings. As the *M*Ti-DLC2 coating showed the highest hardness, reduced modulus, and toughness values, it also showed the highest residual stress value. Increased residual stresses are often considered detrimental for such coatings, but Kovacı et al. [68] showed in their work on DLC coatings that higher values of compressive residual stress can help to inhibit the initiation and propagation of cracks in the coatings under loading.

Fig. 13 shows optical images of the scratch tests of the coatings on the M2 substrates. The adhesive failure (Lc2) values are indicated for each coating.

All the coatings had higher values of adhesion than that of pure DLC. However, the monolayer coatings presented higher values (around 23.5 N) than the multilayer ones (from 16.7 to 20.2 N). Adhesion of the DLC coatings depends on the residual stresses [48] (inverse relationship) but also on the presence of dopants and their physical properties and concentrations. If monolayer and multilayer coatings with identical concentrations of titanium are compared, it can be seen that the latter presented higher compressive stress values, which explains their lower Lc2 values. Concerning the influence of Ti on the adhesion of these coatings, the results indicate a decrease in adhesion as the concentration of titanium increases, in particular for the multilayer coatings because of the irregular distribution of Ti in them.

Fig. 13. Lc2 adhesive failure of the *m*Ti-DLC and *M*Ti-DLC coatings on the M2 substrates.

4. Conclusions

New nanometre scale multilayer magnetron sputtered Ti-DLC/DLC coatings with improved mechanical properties were successfully deposited by non-reactive direct current magnetron sputtering with two different rotational speeds of the substrate holder (12 and 1 rpm).

The mean periods between the DLC and Ti-DLC layers were 0.4 and 5 nm for the monolayer and multilayer coatings, respectively.

All the coatings were mainly amorphous with a columnar structure and a cauliflower-like granular surface morphology. Significant Ti concentration fluctuations were observed for the multilayer coatings (the higher period between layers).

Due to the induced graphitisation in the sp^3 bonded carbon, the sp^2/sp^3 ratio of the multilayer coatings increased as the concentration of Ti rose.

The multilayer coatings showed improved mechanical properties (up to 33 % improvement in hardness and up to 25 % improvement in elastic modulus) compared to the equivalent monolayer coatings. Among all the Ti-doped DLC coatings, the multilayer one with 5.9 at. % of Ti deposited at 1 rpm presented mechanical properties with the highest values, similar to the ones of pure DLC. Finally, it can be stated from the results obtained that, through the deposition of alternating nanometric layers of pure DLC and Ti-doped DLC, it is possible to increase the performance of this type of coatings.

Declaration of competing interest

The authors declare that they have no known competing financial interests or personal relationships that could have appeared to influence the work reported in this paper.

Data availability

Data will be made available on request.

Acknowledgements

This work is supported and funded by the European Network for Joint Doctoral-Level Training in Green Tribology – Horizon 2020 - GreenTRIBOS Project no. 860246.

This research is also sponsored by national funds through FCT – Fundação para a Ciência e a Tecnologia, under the projects UIDB/00285/2020 and LA/P/0112/2020.

The authors thank Professor Joao Carlos Oliveira from Department of Mechanical Engineering, University of Coimbra for performing the RBS-ERDA and NEXAFS analysis of the selected coatings.

The authors thank Mrs. Zabeada Aslam and Mr. Stuart Micklethwaite from Leeds Electron Microscopy and Spectroscopy Centre (LEMAS), University of Leeds for their helpful assistance for the FIB and TEM tests. The authors are grateful for the facility access support by the Engineering and Physical Sciences Research Council (EPSRC, Grants No. EP/S030476/1 and EP/R02524X/1) in the UK.

We also acknowledge support from the Henry Royce Institute (EPSRC grants: EP/P022464/1, EP/R00661X/1), which funded the VXSF Facilities (https://engineering.leeds.ac.uk/vxsf) within the Bragg Centre for Materials Research at Leeds.

References

[1] Y.C. Ean, Y.-J. Jang, J.-K. Kim, W.L. Yun Hsien, N.J. Siambun, S.-S. Kim, Effect of substrate bias on the tribological behavior of ta-C coating prepared by filtered cathodic vacuum arc, Int. J. Precis. Eng. Manuf. 18 (2017) 779–784, https://doi.org/10.1007/s12541-017-0093-5.

[2] S. Prawer, K.W. Nugent, Y. Lifshitz, G.D. Lempert, E. Grossman, J. Kulik, I. Avigal, R. Kalish, Systematic variation of the Raman spectra of DLC films as a function of sp^2:sp^3 composition, Diam. Relat. Mater. 5 (1996) 433–438, https://doi.org/10.1016/0925-9635(95)00363-0.

[3] Y.-H. Lin, H.-D. Lin, C.-K. Liu, M.-W. Huang, J.-R. Chen, H.C. Shih, Structure and characterization of the multilayered Ti-DLC films by FCVA, Diam. Relat. Mater. 19 (2010) 1034–1039, https://doi.org/10.1016/j.diamond.2010.02.014.

[4] J.-B. Wu, J.-J. Chang, M.-Y. Li, M.-S. Leu, A.-K. Li, Characterization of diamond-like carbon coatings prepared by pulsed bias cathodic vacuum arc deposition, Thin Solid Films 516 (2007) 243–247, https://doi.org/10.1016/j.tsf.2007.06.134.

[5] P.W. Shum, K.Y. Li, Z.F. Zhou, Preliminary study of the mechanical and tribological properties of diamond-like carbon films prepared on steel substrates by filtered cathodic vacuum arc deposition, in: D. Dowson, M. Priest, G. Dalmaz, A. A. Lubrecht (Eds.), Bound, Elsevier, Mix. Lubr, 2002, pp. 265–269, https://doi.org/10.1016/S0167-8922(02)80030-X.

[6] Y. Wang, X. Zhang, X. Wu, H. Zhang, X. Zhang, Structural and mechanical properties of amorphous carbon films deposited by the dual plasma technique, J. Univ. Sci. Technol. Beijing, Miner. Metall. Mater. 15 (2008) 622–626, https://doi.org/10.1016/S1005-8850(08)60116-4.

[7] Y. Shen, J. Luo, B. Liao, L. Chen, X. Zhang, Y. Zhao, P. Pang, X. Zeng, Enhanced anti-tribocorrosion performance of Ti-DLC coatings deposited by filtered cathodic vacuum arc with the optimization of bias voltage, Coatings 12 (2022), https://doi.org/10.3390/coatings12050697.

[8] P. Písařík, J. Mikšovský, J. Remsa, J. Zemek, Z. Tolde, M. Jelínek, Diamond-like carbon prepared by pulsed laser deposition with ion bombardment: physical properties, Appl. Phys. A Mater. Sci. Process. 124 (2018) 85, https://doi.org/10.1007/s00339-017-1501-5.

[9] J. Bulír, M. Novotný, M. Jelínek, T. Kocourek, V. Studnička, Plasma study and deposition of DLC/TiC/Ti multilayer structures using technique combining pulsed laser deposition and magnetron sputtering, Surf. Coat. Technol. 200 (2005) 708–711, https://doi.org/10.1016/j.surfcoat.2005.01.087.

[10] Q. Wei, A.K. Sharma, J. Sankar, J. Narayan, Mechanical properties of diamond-like carbon composite thin films prepared by pulsed laser deposition, Compos. Part B Eng. 30 (1999) 675–684, https://doi.org/10.1016/S1359-8368(99)00035-9.

[11] M. Jelínek, J. Zemek, T. Kocourek, J. Remsa, J. Mikšovský, P. Písařík, K. Jurek, Z. Tolde, M. Trávníčková, M. Vandrovcová, E. Filová, Dual laser deposition of Ti: DLC composite for implants, Laser Phys. 26 (2016) 105605, https://doi.org/10.1088/1054-660X/26/10/105605.

[12] T. Fu, Z.F. Zhou, Y.M. Zhou, X.D. Zhu, Q.F. Zeng, C.P. Wang, K.Y. Li, J. Lu, Mechanical properties of DLC coating sputter deposited on surface nanocrystallized 304 stainless steel, Surf. Coat. Technol. 207 (2012) 555–564, https://doi.org/10.1016/j.surfcoat.2012.07.076.

[13] V.Y. Kulikovsky, F. Fendrych, L. Jastrabik, D. Chvostova, Study of formation and some properties of Ti-C:H films prepared by d.c. magnetron sputtering, Surf. Coat. Technol. 91 (1997) 122–130, https://doi.org/10.1016/S0257-8972(96)03146-5.

[14] V.Y. Kulikovsky, F. Fendrych, L. Jastrabik, D. Chvostova, L. Soukup, J. Pridal, F. Franc, The mechanical and tribological properties of magnetron sputtered Ti–C:H coatings, Surf. Coat. Technol. 102 (1998) 81–89, https://doi.org/10.1016/S0257-8972(97)00568-9.

[15] D. Liu, P. Zhang, L. Meng, C. Ruan, Y. Liang, J. Tu, Structure, mechanical properties and tribological behavior of sp^2-C:Ti/sp^3-C:Ti multilayer films deposited by magnetron sputtering, Diam. Relat. Mater. 125 (2022) 108963, https://doi.org/10.1016/j.diamond.2022.108963.

[16] R.L. Li, J.P. Tu, C.F. Hong, D.G. Liu, D.H. Zhou, H.L. Sun, Microstructure and tribological properties of Ti-contained amorphous carbon film deposited by DC magnetron sputtering, J. Appl. Phys. 106 (2009) 123508, https://doi.org/10.1063/1.3272018.

[17] C. Chen, W. Tang, X. Li, W. Wang, C. Xu, Structure and cutting performance of Ti-DLC films prepared by reactive magnetron sputtering, Diam. Relat. Mater. 104 (2020) 107735, https://doi.org/10.1016/j.diamond.2020.107735.

[18] W.Q. Bai, L.L. Li, X.L. Wang, F.F. He, D.G. Liu, G. Jin, J.P. Tu, Effects of Ti content on microstructure, mechanical and tribological properties of Ti-doped amorphous carbon multilayer films, Surf. Coat. Technol. 266 (2015) 70–78, https://doi.org/10.1016/j.surfcoat.2015.02.024.

[19] D. Hofmann, S. Kunkel, K. Bewilogua, R. Wittorf, From DLC to Si-DLC based layer systems with optimized properties for tribological applications, Surf. Coat. Technol. 215 (2013) 357–363, https://doi.org/10.1016/j.surfcoat.2012.06.094.

[20] J.A. Santiago, I. Fernández-Martínez, T. Kozák, J. Capek, A. Wennberg, J. M. Molina-Aldareguia, V. Bellido-González, R. González-Arrabal, M.A. Monclús, The influence of positive pulses on HiPIMS deposition of hard DLC coatings, Surf. Coat. Technol. 358 (2019) 43–49, https://doi.org/10.1016/j.surfcoat.2018.11.001.

[21] S. Majeed, K. Siraj, S. Naseem, M.F. Khan, M. Irshad, H. Faiz, A. Mahmood, Structural and optical properties of gold-incorporated diamond-like carbon thin films deposited by RF magnetron sputtering, Mater. Res. Express. 4 (2017) 76403, https://doi.org/10.1088/2053-1591/aa7430.

[22] J. Vetter, 60 years of DLC coatings: historical highlights and technical review of cathodic arc processes to synthesize various DLC types, and their evolution for industrial applications, Surf. Coat. Technol. 257 (2014) 213–240, https://doi.org/10.1016/j.surfcoat.2014.08.017.

[23] R. Maheswaran, D.J. Thiruvadigal, C. Gopalakrishnan, Thermal instability of DLC film surface morphology - an AFM study, AIP Conf. Proc. 1447 (2012) 789–790, https://doi.org/10.1063/1.4710240.

[24] E. Byon, J.-K. Kim, J.-J. Rha, S.-C. Kwon, Z. Mu, C. Liu, G. Li, Effect of metal ion implantation on thermal instability of diamond-like carbon films, Surf. Coat. Technol. 201 (2007) 6670–6673, https://doi.org/10.1016/j.surfcoat.2006.09.063.

[25] J. Peng, J. Huang, X. Qiu, Y. Xiao, Friction and wear performance of hydrogenated diamond-like coatings with non-metal element complex dopants against alumina in ambient air, Wear 514–515 (2023) 204571, https://doi.org/10.1016/j.wear.2022.204571.

[26] M. Kalin, J. Vižintin, Differences in the tribological mechanisms when using non-doped, metal-doped (Ti, WC), and non-metal-doped (Si) diamond-like carbon against steel under boundary lubrication, with and without oil additives, Thin Solid Films 515 (2006) 2734–2747, https://doi.org/10.1016/j.tsf.2006.03.034.

[27] P.P. Jing, Y.H. Su, Y.X. Li, W.L. Liang, Y.X. Leng, Mechanism of protein biofilm formation on Ag-DLC films prepared for application in joint implants, Surf. Coat. Technol. 422 (2021) 127553, https://doi.org/10.1016/j.surfcoat.2021.127553.

[28] P. Wongpanya, N. Pintitraratibodee, K. Thumanu, C. Euaruksakul, Improvement of corrosion resistance and biocompatibility of 316L stainless steel for joint replacement application by Ti-doped and Ti-interlayered DLC films, Surf. Coat. Technol. 425 (2021) 127734, https://doi.org/10.1016/j.surfcoat.2021.127734.

[29] J.A. Santiago, I. Fernández-Martínez, J.C. Sánchez-López, T.C. Rojas, A. Wennberg, V. Bellido-González, J.M. Molina-Aldareguia, M.A. Monclús, R. González-Arrabal, Tribomechanical properties of hard Cr-doped DLC coatings deposited by low-frequency HiPIMS, Surf. Coat. Technol. 382 (2020) 124899, https://doi.org/10.1016/j.surfcoat.2019.124899.

[30] S. Wan, L. Wang, Q. Xue, Super-hydrophilic properties of TiO_2–DLC nanocomposite films fabricated by the simple electrochemical process, Appl. Surf. Sci. 257 (2011) 10000–10004, https://doi.org/10.1016/j.apsusc.2011.06.127.

[31] J.C. Sánchez-López, A. Fernández, Doping and alloying effects on DLC coatings, in: C. Donnet, A. Erdemir (Eds.), Tribol. Diamond-like Carbon Film. Fundam. Appl, Springer US, Boston, MA, 2008, pp. 311–338, https://doi.org/10.1007/978-0-387-49891-1_12.

[32] G. Ma, S. Gong, G. Lin, L. Zhang, G. Sun, A study of structure and properties of Ti-doped DLC film by reactive magnetron sputtering with ion implantation, Appl. Surf. Sci. 258 (2012) 3045–3050, https://doi.org/10.1016/j.apsusc.2011.11.034.

[33] L. Qiang, B. Zhang, Y. Zhou, J. Zhang, Improving the internal stress and wear resistance of DLC film by low content Ti doping, Solid State Sci. 20 (2013) 17–22, https://doi.org/10.1016/j.solidstatesciences.2013.03.003.

[34] J. Barriga, M. Kalin, K. Van Acker, K. Vercammen, A. Ortega, L. Leiaristi, Tribological performance of titanium doped and pure DLC coatings combined with a synthetic bio-lubricant, Wear 261 (2006) 9–14, https://doi.org/10.1016/j.wear.2005.09.004.

[35] X. Feng, Y. Xia, Tribological properties of Ti-doped DLC coatings under ionic liquids lubricated conditions, Appl. Surf. Sci. 258 (2012) 2433–2438, https://doi.org/10.1016/j.apsusc.2011.10.066.

[36] Z.Y. Zhang, X.C. Lu, J. Bin Luo, T.M. Shao, T. Qing, C.H. Zhang, Preparation and tribological properties of DLC/Ti film by pulsed laser arc deposition, Chin. Phys. 15 (2006) 2697–2705, https://doi.org/10.1088/1009-1963/15/11/039.

[37] Z. Xu, H. Sun, Y.X. Leng, X. Li, W. Yang, N. Huang, Effect of modulation periods on the microstructure and mechanical properties of DLC/TiC multilayer films deposited by filtered cathodic vacuum arc method, Appl. Surf. Sci. 328 (2015) 319–324, https://doi.org/10.1016/j.apsusc.2014.12.041.

[38] D. Sheeja, B.K. Tay, X. Shi, S.P. Lau, C. Daniel, S.M. Krishnan, L.N. Nung, Mechanical and tribological characterization of diamond-like carbon coatings on orthopedic materials, Diam. Relat. Mater. 10 (2001) 1043–1048, https://doi.org/10.1016/S0925-9635(00)00413-1.

[39] Z. Xu, Y.J. Zheng, F. Jiang, Y.X. Leng, H. Sun, N. Huang, The microstructure and mechanical properties of multilayer diamond-like carbon films with different modulation ratios, Appl. Surf. Sci. 264 (2013) 207–212, https://doi.org/10.1016/j.apsusc.2012.10.003.

[40] Y. Ye, Y. Wang, X. Ma, D. Zhang, L. Wang, X. Li, Tribocorrosion behaviors of multilayer PVD DLC coated 304L stainless steel in seawater, Diam. Relat. Mater. 79 (2017) 70–78, https://doi.org/10.1016/j.diamond.2017.09.002.

[41] D.-W. Kim, K.-W. Kim, Effects of sliding velocity and normal load on friction and wear characteristics of multi-layered diamond-like carbon (DLC) coating prepared by reactive sputtering, Wear 297 (2013) 722–730, https://doi.org/10.1016/j.wear.2012.10.009.

[42] J. Lomon, T. Saisopa, P. Poolcharuansin, N. Pasaja, A. Chingsungnoen, R. Supruangnet, H. Nakajima, N. Chanlek, P. Songsiriritthigul, Effect of surface contamination on XANES analysis of DLC films, Radiat. Phys. Chem. 171 (2020) 108752, https://doi.org/10.1016/j.radphyschem.2020.108752.

[43] F. Mangolini, Z. Li, M.A. Marcus, R. Schneider, M. Dienwiebel, Quantification of the carbon bonding state in amorphous carbon materials: a comparison between EELS and NEXAFS measurements, Carbon N. Y. 173 (2021) 557–564, https://doi.org/10.1016/j.carbon.2020.11.021.

[44] A. Mezzi, S. Kaciulis, Surface investigation of carbon films: from diamond to graphite, Surf. Interface Anal. 42 (2010) 1082–1084, https://doi.org/10.1002/sia.3348.

[45] C.A. Charitidis, Nanomechanical and nanotribological properties of carbon-based thin films: a review, Int. J. Refract. Met. Hard Mater. 28 (2010) 51–70, https://doi.org/10.1016/j.ijrmhm.2009.08.003.

[46] S. Kosarieh, A. Morina, J. Flemming, E. Lainé, A. Neville, Wear mechanisms of hydrogenated DLC in oils containing MoDTC, Tribol. Lett. 64 (2016) 4, https://doi.org/10.1007/s11249-016-0737-0.

[47] C.A. Charitidis, S. Logothetidis, Effects of normal load on nanotribological properties of sputtered carbon nitride films, Diam. Relat. Mater. 14 (2005) 98–108, https://doi.org/10.1016/j.diamond.2004.07.022.

[48] X. Sui, J. Liu, S. Zhang, J. Yang, J. Hao, Microstructure, mechanical and tribological characterization of CrN/DLC/Cr-DLC multilayer coating with improved adhesive wear resistance, Appl. Surf. Sci. 439 (2018) 24–32, https://doi.org/10.1016/j.apsusc.2017.12.266.

[49] S.T. Gonczy, N. Randall, An ASTM standard for quantitative scratch adhesion testing of thin, hard ceramic coatings, Int. J. Appl. Ceram. Technol. 2 (2005) 422–428, https://doi.org/10.1111/j.1744-7402.2005.02043.x.

[50] S. Shiri, P. Ashtijoo, A. Odeshi, Q. Yang, Evaluation of stoney equation for determining the internal stress of DLC thin films using an optical profiler, Surf. Coat. Technol. 308 (2016) 98–100, https://doi.org/10.1016/j.surfcoat.2016.07.098.

[51] F. Ferreira, R. Serra, A. Cavaleiro, J. Oliveira, Diamond-like carbon coatings deposited by deep oscillation magnetron sputtering in Ar-Ne discharges, Diam. Relat. Mater. 98 (2019) 107521, https://doi.org/10.1016/j.diamond.2019.107521.

[52] S. Calderon Velasco, A. Cavaleiro, S. Carvalho, Functional properties of ceramic-Ag nanocomposite coatings produced by magnetron sputtering, Prog. Mater. Sci. 84 (2016) 158–191, https://doi.org/10.1016/j.pmatsci.2016.09.005.

[53] W. Dai, A. Wang, Deposition and properties of Al-containing diamond-like carbon films by a hybrid ion beam sources, J. Alloys Compd. 509 (2011) 4626–4631, https://doi.org/10.1016/j.jallcom.2011.01.132.

[54] A.F. Yetim, H. Kovacı, A.E. Kasapoğlu, Y.B. Bozkurt, A. Çelik, Influences of Ti, Al and V metal doping on the structural, mechanical and tribological properties of DLC films, Diam. Relat. Mater. 120 (2021) 108639, https://doi.org/10.1016/j.diamond.2021.108639.

[55] H. Cao, X. Ye, H. Li, F. Qi, Q. Wang, X. Ouyang, N. Zhao, B. Liao, Microstructure, mechanical and tribological properties of multilayer Ti-DLC thick films on Al alloys by filtered cathodic vacuum arc technology, Mater. Des. 198 (2021) 109320, https://doi.org/10.1016/j.matdes.2020.109320.

[56] L. Qiang, K. Gao, L. Zhang, J. Wang, B. Zhang, J. Zhang, Further improving the mechanical and tribological properties of low content Ti-doped DLC film by W incorporating, Appl. Surf. Sci. 353 (2015) 522–529, https://doi.org/10.1016/j.apsusc.2015.06.040.

[57] Y. Zhou, L. Li, T. Hu, Q. Wang, W. Shao, L. Rao, X. Xing, Q. Yang, Role of TiC nanocrystalline and interface of TiC and amorphous carbon on corrosion mechanism of titanium doped diamond-like carbon films: exploration by experimental and first principle calculation, Appl. Surf. Sci. 542 (2021) 148740, https://doi.org/10.1016/j.apsusc.2020.148740.

[58] A. Saikubo, N. Yamada, K. Kanda, S. Matsui, T. Suzuki, K. Niihara, H. Saitoh, Comprehensive classification of DLC films formed by various methods using

NEXAFS measurement, Diam. Relat. Mater. 17 (2008) 1743–1745, https://doi.org/10.1016/j.diamond.2008.01.095.
[59] K. Kanda, K. Fukuda, K. Kidena, R. Imai, M. Niibe, S. Fujimoto, K. Yokota, M. Tagawa, Hyperthermal atomic oxygen beam irradiation effect on the Ti-containing DLC film, Diam. Relat. Mater. 41 (2014) 49–52, https://doi.org/10.1016/j.diamond.2013.10.006.
[60] Y.J. Jo, T.F. Zhang, M.J. Son, K.H. Kim, Synthesis and electrochemical properties of Ti-doped DLC films by a hybrid PVD/PECVD process, Appl. Surf. Sci. 433 (2018) 1184–1191, https://doi.org/10.1016/j.apsusc.2017.10.151.
[61] P. Mérel, M. Tabbal, M. Chaker, S. Moisa, J. Margot, Direct evaluation of the sp^3 content in diamond-like-carbon films by XPS, Appl. Surf. Sci. 136 (1998) 105–110, https://doi.org/10.1016/S0169-4332(98)00319-5.
[62] J. Robertson, Diamond-like amorphous carbon, Mater. Sci. Eng. R. Rep. 37 (2002) 129–281, https://doi.org/10.1016/S0927-796X(02)00005-0.
[63] M. Evaristo, R. Azevedo, C. Palacio, A. Cavaleiro, Influence of the silicon and oxygen content on the properties of non-hydrogenated amorphous carbon coatings, Diam. Relat. Mater. 70 (2016) 201–210, https://doi.org/10.1016/j.diamond.2016.10.024.
[64] B. Feng, D.M. Cao, W.J. Meng, L.E. Rehn, P.M. Baldo, G.L. Doll, Probing for mechanical and tribological anomalies in the TiC/amorphous hydrocarbon nanocomposite coating system, Thin Solid Films 398–399 (2001) 210–216, https://doi.org/10.1016/S0040-6090(01)01427-4.
[65] J. Jiang, Q. Wang, H. Huang, Y. Wang, X. Zhang, J. Hao, Microstructure and property changes induced by substrate rotation in titanium/silicon dual-doped a-C:H films deposited by mid-frequency magnetron sputtering, Surf. Coat. Technol. 240 (2014) 419–424, https://doi.org/10.1016/j.surfcoat.2013.12.067.
[66] Y.L. Kao, G.C. Tu, C.A. Huang, T.T. Liu, A study on the hardness variation of α- and β-pure titanium with different grain sizes, Mater. Sci. Eng. A 398 (2005) 93–98, https://doi.org/10.1016/j.msea.2005.03.004.
[67] P. Xu, J.J. Li, Q. Wang, Z.L. Wang, C.Z. Gu, Z. Cui, Improving mechanical properties of amorphous carbon nitride films by titanium doping, J. Appl. Phys. 101 (2007) 14312, https://doi.org/10.1063/1.2404797.
[68] H. Kovacı, A.F. Yetim, Ö. Baran, A. Çelik, Fatigue crack growth behavior of DLC coated AISI 4140 steel under constant and variable amplitude loading conditions, Surf. Coat. Technol. 304 (2016) 316–324, https://doi.org/10.1016/j.surfcoat.2016.07.045.